Inorganic Chemistry

Article

pubs.acs.org/IC

Electron-Deficient Ternary and Quaternary Pnictides $Rb_4Zn_7As_7$, $Rb_4Mn_{3.5}Zn_{3.5}Sb_7$, $Rb_7Mn_{12}Sb_{12}$, and $Rb_7Mn_4Cd_8Sb_{12}$ with Corrugated Anionic Layers

Mansura Khatun, Stanislav S. Stoyko, and Arthur Mar*

Department of Chemistry, University of Alberta, Edmonton, Alberta, Canada T6G 2G2

Supporting Information

ABSTRACT: The ternary pnictides $Rb_4Zn_7As_7$ and $Rb_7Mn_{12}Sb_{12}$ and their quaternary derivatives $Rb_4Mn_{3.5}Zn_{3.5}Sb_7$ and $Rb_7Mn_4Cd_8Sb_{12}$ have been prepared by reactions of the elements at 600 °C. They crystallize in two new structure types: orthorhombic $Rb_4Zn_7As_7$-type (space group *Cmcm*, $Z = 4$; $a = 4.1883(4)$ Å, $b = 24.844(2)$ Å, $c = 17.6056(17)$ Å for $Rb_4Zn_7As_7$; $a = 4.3911(8)$ Å, $b = 26.546(5)$ Å, $c = 18.743(4)$ Å for $Rb_4Mn_{3.5}Zn_{3.5}Sb_7$) and monoclinic $Rb_7Mn_{12}Sb_{12}$-type (space group *C*2/*m*, $Z = 2$; $a = 26.544(12)$ Å, $b = 4.448(2)$ Å, $c = 16.676(8)$ Å, $\beta = 103.183(8)°$ for $Rb_7Mn_{12}Sb_{12}$; $a = 27.009(4)$ Å, $b = 4.5752(7)$ Å, $c = 16.727(3)$ Å, $\beta = 103.221(2)°$ for $Rb_7Mn_4Cd_8Sb_{12}$). These related structures contain corrugated anionic layers built up by connecting ribbons of edge-sharing tetrahedra in a zigzag-like manner with chains of Mn-centered square pyramids located at the hinges. Homoatomic pnicogen−pnicogen bonding occurs in the form of Pn_2 pairs. The compounds are formally deficient by one electron per formula unit, as confirmed by band structure calculations which reveal the location of the Fermi level just below a small gap in $Rb_4Zn_7As_7$ or a pseudogap in $Rb_7Mn_{12}Sb_{12}$.

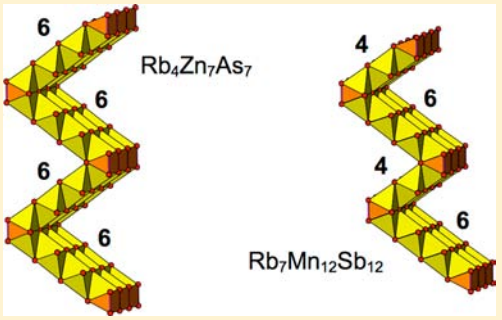

INTRODUCTION

Ternary arsenides and antimonides A−M−Pn containing an electropositive metal A and a d-block element M represent a growing category of solid-state compounds useful for materials applications. An important subset comprises charge-balanced Zintl phases forming isostructural series in which the M substituent has a d^5 or d^{10} configuration (M = Mn, Zn, Cd) and can be extended to include p-block metalloids (M = Al, Ga, In).[1] Among numerous examples, perhaps the most well-known is the $A_{14}MPn_{11}$ series (A = alkaline-earth and divalent rare-earth metal) adopting the $Ca_{14}AlSb_{11}$-type structure; in particular, $Yb_{14}MnSb_{11}$ has been examined extensively for its thermoelectric, magnetoresistive, and other transport properties.[2−4] Relatively fewer examples are known in which A is an alkali metal, but they also show interesting properties. They range from equiatomic phases AMPn (A = Li−Cs; M = Mn, Zn, Cd; Pn = As, Sb) adopting simple structures such as cubic MgAgAs- or tetragonal PbFCl-type,[5−8] to complex phases $A_8M_{18}Pn_{28}$ (A = K, Rb, Cs; M = Zn, Cd; Pn = As, Sb) crystallizing in clathrate structures.[9,10] LiZnSb and $A_8M_{18}Pn_{28}$ have been assessed for their thermoelectric properties;[10−13] KHgSb may be a suitable candidate as a weak topological insulator;[14] and Mn-doped LiZnAs is a dilute half-metallic ferromagnetic semiconductor with potential applications in spintronics.[15]

Further investigations within these alkali-metal-containing systems have led to the discovery of ternary pnictides $A_2M_5Pn_4$ (A = K, Rb, Cs; M = Zn, Cd; Pn = As, Sb),[9,16−19] RbM_4As_3 (M = Zn, Cd),[17] and Cs_4MAs_{14} (M = Zn, Cd),[20] as well as quaternary arsenides $AM_{1.5}Tt_{0.5}As_2$ (A = Na, K, Rb; M = Zn, Cd; Tt = Si, Ge, Sn),[21] $A_2A'CdSb_2$ (A = Na, K; A′ = Ca, Sr, Ba, Eu, Yb),[22] and $KA'_2Cd_2Sb_3$ (A′ = Ca, Sr, Ba, Eu, Yb).[23] In continuation of these efforts, we report here the preparation of four new rubidium-containing pnictides: $Rb_4Zn_7As_7$, $Rb_4Mn_{3.5}Zn_{3.5}Sb_7$, $Rb_7Mn_{12}Sb_{12}$, and $Rb_7Mn_4Cd_8Sb_{12}$. Their related crystal structures illustrate a principle for connecting edge-sharing tetrahedra to generate corrugated anionic layers not observed previously. Their electronic structures are also examined through band structure calculations, providing support for a one-electron deficiency observed in these compounds.

EXPERIMENTAL SECTION

Synthesis. Starting materials were Rb pieces (99.75%, Alfa-Aesar), Mn powder (99.6%, Alfa-Aesar), Zn shot (99.99%, Aldrich), Cd shot (99.95%, Alfa-Aesar), As lumps (99.999%, Alfa-Aesar), and Sb ingots (99.999%, Alfa-Aesar). All reagents and products were handled within an argon-filled glovebox. $Rb_7Mn_{12}Sb_{12}$ was first identified in the course of attempts to prepare "$A_2Mn_5Pn_4$" (A = K, Rb; Pn = As, Sb). Substitution of the d-block component with Cd or Zn then led to the isostructural compound $Rb_7Mn_4Cd_8Sb_{12}$ as well as the different phase $Rb_4Mn_{3.5}Zn_{3.5}Sb_7$. Further substitution of the pnicogen component eventually revealed the arsenide $Rb_4Zn_7As_7$. The title compounds were prepared from stoichiometric mixtures of the elements, which were loaded into alumina crucibles placed within fused-silica tubes. The tubes were evacuated and sealed; they were then heated to 600 °C

Received: July 22, 2013
Published: October 11, 2013

   dx.doi.org/10.1021/ic401887b | *Inorg. Chem.* 2013, 52, 12682−12690

over 2 d, kept at this temperature for 10 d, and cooled to room temperature over 2 d. The fused-silica tubes were not attacked, but became slightly turbid, likely a result of partial vaporization of Rb during the heat treatment. The resulting products were air-sensitive, visibly tarnishing within minutes, and were examined under paraffin oil. Products were analyzed by powder X-ray diffraction (XRD) patterns collected on an Inel diffractometer equipped with a curved position-sensitive detector (CPS 120) and a Cu Kα_1 radiation source operated at 40 kV and 20 mA. These XRD patterns suffered from a high background as a result of contributions from the paraffin oil and X-ray fluorescence from the Mn component within the samples. However, the title compounds generally constituted the major phase, as suggested by a representative XRD pattern for $Rb_7Mn_{12}Sb_{12}$ (Figure S1 in Supporting Information). Crystals of these compounds grew as thin needles (Figure S2 in Supporting Information). The chemical compositions of crystals selected for single-crystal X-ray diffraction experiments were determined by energy-dispersive X-ray (EDX) analysis on a JEOL JSM-6010LA scanning electron microscope and were in good agreement with expectations (Table S1 in Supporting Information). Attempts to prepare other permutations within the series $Rb_4M_7Pn_7$, $Rb_4M_{3.5}M'_{3.5}Pn_7$, $Rb_7M_{12}Pn_{12}$, and $Rb_7M_4M'_8Pn_{12}$ (M, M′ = Mn, Zn, Cd; Pn = As, Sb) under the same synthetic conditions as above were unsuccessful.

Structure Determination. Single crystals were mounted within small droplets of paraffin oil on glass fibers and placed under a cold nitrogen gas stream on a Bruker PLATFORM diffractometer equipped with a SMART APEX II CCD detector and a Mo Kα radiation source. Intensity data were collected at −100 °C using ω scans with a scan width of 0.3° and an exposure time of 12−20 s per frame at 6−7 different ϕ angles. Face-indexed numerical absorption corrections were applied. Structure solution and refinement were carried out with use of the SHELXTL (version 6.12) program package.[24] Full crystallographic details and interatomic distances are listed in Tables S2−S4 in Supporting Information. Table 1 gives abbreviated details of the crystallographic data. Table 2 listing atomic coordinates and equivalent isotropic displacement parameters is provided in the main text to facilitate discussion of the structure determinations below. Table 3 lists ranges of interatomic distances.

Table 1. Crystallographic Data for $Rb_4Zn_7As_7$, $Rb_4Mn_{3.5}Zn_{3.5}Sb_7$, $Rb_7Mn_{12}Sb_{12}$, and $Rb_7Mn_4Cd_8Sb_{12}$

	$Rb_4Zn_7As_7$	$Rb_4Mn_{3.4(1)}Zn_{3.6(1)}Sb_7$	$Rb_7Mn_{12}Sb_{12}$	$Rb_7Mn_{4.2(1)}Cd_{7.8(1)}Sb_{12}$
fw (amu)	1323.91	1615.22	2718.57	3178.25
space group	*Cmcm* (No. 63)	*Cmcm* (No. 63)	*C*2/*m* (No. 12)	*C*2/*m* (No. 12)
a (Å)	4.1883(4)	4.3911(8)	26.544(12)	27.009(4)
b (Å)	24.844(2)	26.546(5)	4.448(2)	4.5752(7)
c (Å)	17.6056(17)	18.743(4)	16.676(8)	16.727(3)
β (deg)	90	90	103.183(8)	103.221(2)
V (Å^3)	1831.9(3)	2184.7(7)	1917(2)	2012.2(5)
Z	4	4	2	2
ρ_{calcd} (g cm^{-3})	4.800	4.911	4.710	5.246
T (K)	173(2)	173(2)	173(2)	173(2)
radiation	graphite monochromated Mo Kα, λ = 0.710 73 Å			
μ (mm^{-1})	32.09	23.04	20.91	21.63
$R(F)^a$	0.061	0.034	0.068	0.034
$R_w(F_o^2)^b$	0.161	0.068	0.130	0.065

$^aR(F) = \sum||F_o| - |F_c||/\sum|F_o|$ for $F_o^2 > 2\sigma(F_o^2)$. $^bR_w(F_o^2) = [\sum[w(F_o^2 - F_c^2)^2]/\sum wF_o^4]^{1/2}$; $w^{-1} = [\sigma^2(F_o^2) + (Ap)^2 + Bp]$, where $p = [\max(F_o^2,0) + 2F_c^2]/3$.

On the basis of Laue symmetry, systematic absences, and intensity statistics, the space groups chosen were either *Cmcm* for $Rb_4Zn_7As_7$ and $Rb_4Mn_{3.5}Zn_{3.5}Sb_7$, or *C*2/*m* for $Rb_7Mn_{12}Sb_{12}$ and $Rb_7Mn_4Cd_8Sb_{12}$. In general, structure solution and refinement for the ternary compounds $Rb_4Zn_7As_7$ and $Rb_7Mn_{12}Sb_{12}$ were straightforward, but the treatment of disorder in the quaternary compounds $Rb_4Mn_{3.5}Zn_{3.5}Sb_7$ and $Rb_7Mn_4Cd_8Sb_{12}$ required special attention. In $Rb_4Mn_{3.5}Zn_{3.5}Sb_7$, four sites for the M component were identified. Refinements were performed in which each M site was allowed to be occupied by a mixture of Mn and Zn atoms, with the constraint that the occupancies sum to unity but with no restriction placed on the overall formula. The occupancies converged to 0.22(2) Mn/0.78(2) Zn in M1, 0.60(2) Mn/0.40(2) Zn in M2, and 0.40(2) Mn/0.60(2) Zn in M3; in contrast, M4 tended toward an occupancy of >1.00 Mn (accompanied by a physically meaningless negative Zn occupancy), which we interpret as evidence for this site being exclusively occupied by Mn atoms. If Zn mixing is not allowed in the M4 site, its occupancy converges to 0.999(6) Mn. These refinements are stable and converge to the same occupancies when different starting values are introduced. In a similar manner, six M sites were available in $Rb_7Mn_4Cd_8Sb_{12}$ to be occupied by mixtures of Mn and Cd atoms. Here, the occupancies converged to 0.134(5) Mn/0.866(5) Cd in M1, 0.280(5) Mn/0.720(5) Cd in M2, 0.343(5) Mn/0.657(5) Cd in M3, 0.237(5) Mn/0.763(5) Cd in M4, 0.986(5) Mn/0.014(5) Cd in M5, and 0.106(5) Mn/0.894(5) Cd in M6. The M5 site was thus assigned to be exclusively occupied by Mn atoms. The resulting formulas from these refinements were "$Rb_4Mn_{3.4(1)}Zn_{3.6(1)}Sb_7$" and "$Rb_7Mn_{4.2(1)}Cd_{7.8(1)}Sb_{12}$", which are consistent with the loaded compositions and the EDX analyses. For brevity, we use the simplified formulas $Rb_4Mn_{3.5}Zn_{3.5}Sb_7$ and $Rb_7Mn_4Cd_8Sb_{12}$ in subsequent discussion.

The displacement parameters for atoms in these four structures were reasonable (with U_{eq} values generally ranging from 0.01 to 0.03 Å^2), but they appeared to be somewhat elevated for the Zn4 site (0.051(1) Å^2) and especially the As2 site (0.067(1) Å^2) in $Rb_4Zn_7As_7$. However, the displacement parameters were not significantly reduced when partial occupancy was introduced into these sites (0.043(1) Å^2 for Zn4 at 0.89(1) occupancy and 0.054(1) Å^2 for As2 at 0.85(1) occupancy). Refinements of the occupancies of all other sites confirmed that they are fully occupied. A comparison of the fully stoichiometric model "$Rb_4Zn_7As_7$" and the substoichiometric model "$Rb_4Zn_{6.90(1)}As_{6.70(2)}$" is provided in Table S5 in Supporting Information. Because the agreement factors do improve ($R(F)$ for $F_o^2 > 2\sigma(F_o^2)$ decreasing from 0.0614 to 0.0565) upon introduction of two occupancy parameters, we cannot definitively rule out the substoichiometric model. In both cases, the As2 site exhibits a somewhat elongated displacement ellipsoid, but refinements in which it was split into two sites were unstable. Closer inspection suggests that this feature is likely intrinsic to the structure, given the unusual coordination environments around these atoms, as discussed later.

Atomic positions were standardized with the program STRUCTURE TIDY.[25] Further data, in the form of crystallographic information files (CIFs), are available as Supporting Information or may be obtained from Fachinformationszentrum Karlsruhe, Abt. PROKA, 76344 Eggenstein-Leopoldshafen, Germany (Nos. CSD-426459 to 426462).

Band Structure Calculations. Tight-binding linear muffin tin orbital band structure calculations were performed on $Rb_4Zn_7As_7$ and $Rb_7Mn_{12}Sb_{12}$ within the local density and atomic spheres approximation with use of the Stuttgart TB-LMTO-ASA program (version 4.7).[26] Cell parameters and atomic positions were taken directly from the refined crystal structures. The basis sets included Rb 5s/5p/4d/4f, Mn 4s/4p/3d, Zn 4s/4p/3d, As 4s/4p/4d, and Sb 5s/5p/4d/4f orbitals, with the Rb 5p/4d/4f, As 4d, and Sb 5d/4f orbitals being downfolded. Integrations in reciprocal space were carried out with an improved tetrahedron method over 63 ($Rb_4Zn_7As_7$) or 78 ($Rb_7Mn_{12}Sb_{12}$) irreducible *k* points within the first Brillouin zone.

RESULTS AND DISCUSSION

The four rubidium transition-metal pnictides prepared here belong to two series adopting new orthorhombic ($Rb_4Zn_7As_7$ and $Rb_4Mn_{3.5}Zn_{3.5}Sb_7$ in space group *Cmcm*) and monoclinic ($Rb_7Mn_{12}Sb_{12}$ and $Rb_7Mn_4Cd_8Sb_{12}$ in space group *C*2/*m*) structures, with the ternary compounds conveniently serving as

dx.doi.org/10.1021/ic401887b | Inorg. Chem. 2013, 52, 12682−12690

Table 2. Atomic Coordinates and Equivalent Isotropic Displacement Parameters for $Rb_4Zn_7As_7$, $Rb_4Mn_{3.5}Zn_{3.5}Sb_7$, $Rb_7Mn_{12}Sb_{12}$, and $Rb_7Mn_4Cd_8Sb_{12}$

atom	Wyckoff position	occupancy	x	y	z	U_{eq}[a] (Å^2)
$Rb_4Zn_7As_7$						
Rb1	8*f*	1	0	0.135 77(7)	0.6173(1)	0.0242(4)
Rb2	4*c*	1	0	0.719 12(9)	$^1/_4$	0.0172(4)
Rb3	4*a*	1	0	0	0	0.0345(7)
Zn1	8*f*	1	0	0.148 44(8)	0.1023(1)	0.0210(4)
Zn2	8*f*	1	0	0.282 86(7)	0.5358(1)	0.0134(3)
Zn3	8*f*	1	0	0.571 94(11)	0.1662(1)	0.0374(6)
Zn4	4*c*	1	0	0.006 31(15)	$^1/_4$	0.0509(11)
As1	8*f*	1	0	0.252 45(6)	0.1050(1)	0.0132(3)
As2	8*f*	1	0	0.469 37(10)	0.1829(2)	0.0671(10)
As3	8*f*	1	0	0.610 89(6)	0.0389(1)	0.0147(3)
As4	4*c*	1	0	0.109 90(9)	$^1/_4$	0.0147(4)
$Rb_4Mn_{3.4(1)}$ $Zn_{3.6(1)}Sb_7$						
Rb1	8*f*	1	0	0.137 60(3)	0.615 05(4)	0.0188(2)
Rb2	4*c*	1	0	0.718 50(4)	$^1/_4$	0.0149(2)
Rb3	4*a*	1	0	0	0	0.0229(2)
M1	8*f*	0.22(2) Mn, 0.78(2) Zn	0	0.151 02(4)	0.102 72(5)	0.0165(3)
M2	8*f*	0.59(2) Mn, 0.41(2) Zn	0	0.283 62(4)	0.534 03(5)	0.0132(3)
M3	8*f*	0.40(2) Mn, 0.60(2) Zn	0	0.571 93(4)	0.168 88(5)	0.0169(3)
M4	4*c*	1.00 Mn	0	0.006 59(6)	$^1/_4$	0.0131(3)
Sb1	8*f*	1	0	0.253 51(2)	0.106 77(3)	0.0123(1)
Sb2	8*f*	1	0	0.469 12(2)	0.173 59(3)	0.0151(1)
Sb3	8*f*	1	0	0.610 74(2)	0.038 02(3)	0.0124(1)
Sb4	4*c*	1	0	0.111 46(3)	$^1/_4$	0.0117(1)
$Rb_7Mn_{12}Sb_{12}$						
Rb1	4*i*	1	0.261 48(9)	0	0.2902(1)	0.0203(5)
Rb2	4*i*	1	0.379 33(8)	0	0.1281(1)	0.0217(5)
Rb3	4*i*	1	0.420 81(9)	0	0.4386(1)	0.0263(5)
Rb4	2*b*	1	0	$^1/_2$	0	0.0268(7)
Mn1	4*i*	1	0.099 96(12)	0	0.1983(2)	0.0173(7)
Mn2	4*i*	1	0.125 92(12)	0	0.3826(2)	0.0158(7)
Mn3	4*i*	1	0.220 71(12)	0	0.0400(2)	0.0154(7)
Mn4	4*i*	1	0.289 44(12)	0	0.5408(2)	0.0154(7)
Mn5	4*i*	1	0.545 19(12)	0	0.2896(2)	0.0146(7)
Mn6	4*i*	1	0.665 23(12)	0	0.1226(2)	0.0166(7)
Sb1	4*i*	1	0.004 16(6)	0	0.7985(1)	0.0183(3)
Sb2	4*i*	1	0.021 01(6)	0	0.3790(1)	0.0183(3)
Sb3	4*i*	1	0.115 33(5)	0	0.0442(1)	0.0152(3)
Sb4	4*i*	1	0.184 26(5)	0	0.5387(1)	0.0161(3)
Sb5	4*i*	1	0.651 23(5)	0	0.2915(1)	0.0141(3)
Sb6	4*i*	1	0.769 50(5)	0	0.1230(1)	0.0155(3)
$Rb_7Mn_{4.2(1)}Cd_{7.8(1)}Sb_{12}$						
Rb1	4*i*	1	0.249 92(3)	0	0.288 24(5)	0.0158(2)
Rb2	4*i*	1	0.376 60(3)	0	0.134 14(5)	0.0186(2)
Rb3	4*i*	1	0.419 46(3)	0	0.439 42(6)	0.0217(2)
Rb4	2*b*	1	0	$^1/_2$	0	0.0283(3)
M1	4*i*	0.135(5) Mn, 0.865(5) Cd	0.089 59(3)	0	0.187 21(4)	0.0173(2)
M2	4*i*	0.282(5) Mn, 0.718(5) Cd	0.122 15(3)	0	0.391 83(4)	0.0150(2)
M3	4*i*	0.345(5) Mn, 0.655(5) Cd	0.222 06(3)	0	0.039 47(4)	0.0132(2)
M4	4*i*	0.239(5) Mn, 0.761(5) Cd	0.290 67(3)	0	0.536 68(4)	0.0138(2)
M5	4*i*	1.00 Mn	0.538 03(5)	0	0.292 53(8)	0.0130(2)
M6	4*i*	0.105(5) Mn, 0.895(5) Cd	0.662 81(2)	0	0.116 03(4)	0.0142(2)
Sb1	4*i*	1	0.012 09(2)	0	0.793 52(4)	0.0162(1)
Sb2	4*i*	1	0.015 98(2)	0	0.382 42(3)	0.0151(1)
Sb3	4*i*	1	0.111 47(2)	0	0.032 92(3)	0.0136(1)
Sb4	4*i*	1	0.185 19(2)	0	0.550 02(3)	0.0144(1)
Sb5	4*i*	1	0.643 46(2)	0	0.291 02(3)	0.0113(1)
Sb6	4*i*	1	0.770 67(2)	0	0.129 48(3)	0.0137(1)

[a] U_{eq} is defined as one-third of the trace of the orthogonalized U_{ij} tensor.

dx.doi.org/10.1021/ic401887b | *Inorg. Chem.* 2013, 52, 12682−12690

Table 3. Ranges of Interatomic Distances (Å) for $Rb_4Zn_7As_7$, $Rb_4Mn_{3.5}Zn_{3.5}Sb_7$, $Rb_7Mn_{12}Sb_{12}$, and $Rb_7Mn_4Cd_8Sb_{12}$

	$Rb_4Zn_7As_7$	$Rb_4Mn_{3.5}Zn_{3.5}Sb_7$
Rb1−Pn (CN6)	3.485(1)−3.541(2)	3.633(1)−3.748(1)
Rb2−Pn (CN6)	3.405(1)−3.428(3)	3.590(1)−3.591(1)
Rb3−Pn (CN8)	3.528(1)−3.916(3)	3.738(1)−4.010(1)
M1−Pn (CN4)	2.549(1)−2.772(4)	2.722(1)−2.953(1)
M2−Pn (CN4)	2.576(1)−2.640(2)	2.758(1)−2.806(1)
M3−Pn (CN4)	2.441(3)−2.729(2)	2.660(1)−2.870(1)
M4−Pn (CN5)	2.574(4)−2.574(2)	2.784(2)−2.804(1)
M−M	2.940(2)−3.044(2)	3.041(2)−3.281(1)
Pn2−Pn2	2.363(7)	2.864(1)
	$Rb_7Mn_{12}Sb_{12}$	$Rb_7Mn_4Cd_8Sb_{12}$
Rb1−Sb (CN6)	3.611(2)−3.680(2)	3.644(1)−3.683(1)
Rb2−Sb (CN6)	3.652(2)−3.779(2)	3.650(1)−3.751(1)
Rb3−Sb (CN6)	3.653(3)−3.799(3)	3.672(1)−3.844(1)
Rb4−Sb (CN8)	3.719(2)−4.051(2)	3.720(1)−4.217(1)
M1−Sb (CN4)	2.692(4)−2.872(2)	2.776(1)−3.035(1)
M2−Sb (CN4)	2.709(3)−2.858(2)	2.800(1)−2.975(1)
M3−Sb (CN4)	2.779(2)−2.814(4)	2.877(1)−2.964(1)
M4−Sb (CN4)	2.759(2)−2.880(3)	2.862(1)−3.021(1)
M5−Sb (CN5)	2.808(4)−2.832(2)	2.853(1)−2.874(1)
M6−Sb (CN4)	2.761(2)−2.924(4)	2.865(1)−3.089(1)
M−M	2.993(5)−3.246(3)	3.188(1)−3.412(1)
Sb1−Sb2	2.883(2)	2.866(1)

names of the structure types. There are 3 Rb, 4 M, and 4 Pn sites in the $Rb_4Zn_7As_7$-type structure, and 4 Rb, 6 M, and 6 Pn sites in the $Rb_7Mn_{12}Sb_{12}$-type structure. Viewed down the short crystallographic axis (~4 Å), these closely related structures consist of corrugated anionic layers separated by Rb cations (Figure 1). In $Rb_4Zn_7As_7$, the layers extend parallel to the *ac*-plane and stack along the *b*-direction; in $Rb_7Mn_{12}Sb_{12}$, they extend parallel to the *bc*-plane and stack along the *a*-direction. These layers are built up of M-centered tetrahedra, which share edges to form infinite four- or six-tetrahedra-wide ribbons, as well as M-centered square pyramids, which share opposite edges to form an infinite chain (Figure 2a). The ribbons of tetrahedra are connected in a zigzag-like manner, and the chains of square pyramids are located at the hinges. The layers contain a uniform sequence of six-tetrahedra-wide ribbons in $Rb_4Zn_7As_7$ but an alternating sequence of four- and six-tetrahedra-wide ribbons in $Rb_7Mn_{12}Sb_{12}$ (Figure 2b), resulting in an oblique layer stacking associated with the lower monoclinic symmetry in the latter. Such ribbons, of course, can be considered to be fragments of PbO-type layers of edge-sharing tetrahedra which are common in many structures.[27]

In the quaternary compounds $Rb_4Mn_{3.5}Zn_{3.5}Sb_7$ and $Rb_7Mn_4Cd_8Sb_{12}$, the presence of two different transition metals introduces the possibility of disorder within the tetrahedral or square pyramidal M sites. Structural refinements indicate that the square pyramidal sites are occupied exclusively by Mn atoms in both compounds, whereas the tetrahedral sites are occupied by a mixture of Mn and Zn or Cd atoms. The site distribution within the tetrahedral sites is irregular. In order of decreasing occupancy, the Zn atoms prefer the M1 (0.78), M3 (0.60), and M2 (0.41) tetrahedral sites in $Rb_4Mn_{3.5}Zn_{3.5}Sb_7$. In contrast, the site preference of the Cd atoms is more muted in $Rb_7Mn_4Cd_8Sb_{12}$: M6 (0.90), M1 (0.86), M4 (0.76), M2 (0.72), M3 (0.66). There does not appear to be a simple trend that relates the site distribution to the patterns of tetrahedra within the ribbons (Figure 2b) or size effects as gauged by the

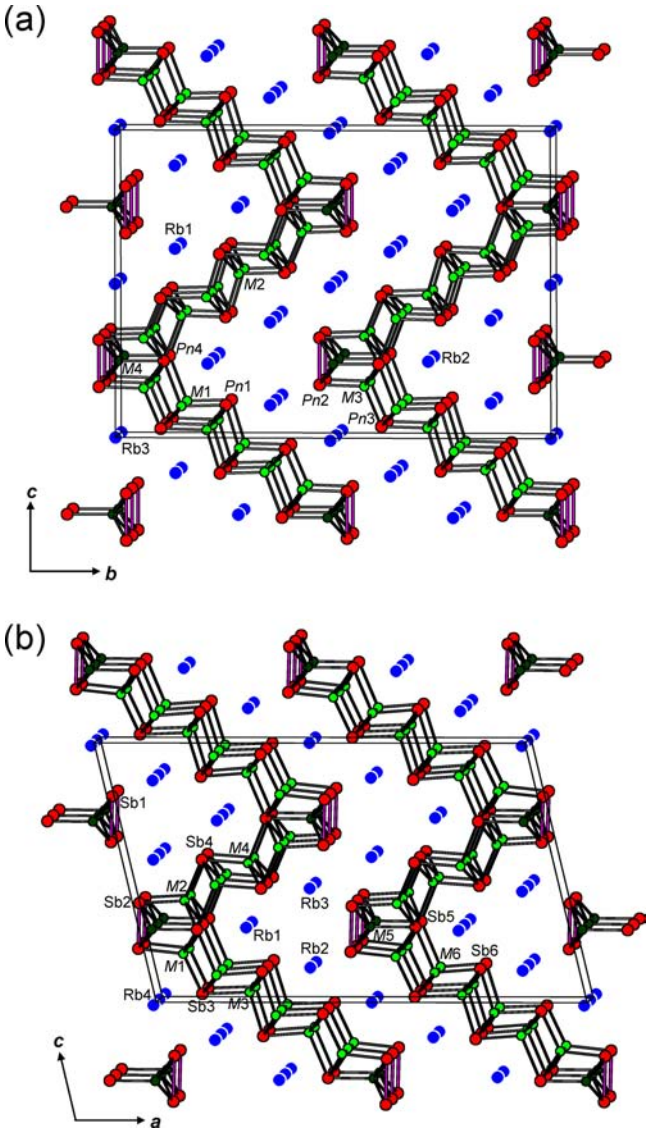

Figure 1. (a) Orthorhombic $Rb_4Zn_7As_7$-type and (b) monoclinic $Rb_7Mn_{12}Sb_{12}$-type structures, viewed down the short-axis directions. The large blue circles are Rb atoms, the small green circles are transition-metal atoms (M = Mn, Zn, Cd), and the medium red circles are pnicogen atoms (Pn = As, Sb).

observed bond distances (Table 2). On the basis of Pauling metallic radii (R_1 of 2.39 Å for Mn, 2.42 Å for Zn, and 2.59 Å for Cd)[28] or other scales of radii, it is difficult to distinguish between the similar-sized Mn and Zn atoms, but it may be possible to identify the larger Cd atoms. In the parent ternary structures ($Rb_4Zn_7As_7$, $Rb_7Mn_{12}Sb_{12}$) as well as in $Rb_4Mn_{3.5}Zn_{3.5}Sb_7$, there is no obvious segregation of M−Pn bond lengths within the tetrahedral or square pyramidal sites. In $Rb_7Mn_4Cd_8Sb_{12}$, the average M−Sb bond length within the square pyramidal site occupied by Mn atoms is only marginally shorter (2.87 Å) compared with those within the tetrahedral sites occupied by a mixture of Mn and Cd atoms (2.89−2.92 Å).

Some of the coordination environments around the Rb atoms are unusual (Figure 3). Although a trigonal prism (CN6) is a common geometry, it becomes highly distorted around Rb1 in the $Rb_4Zn_7As_7$-type structure and around Rb2 and Rb3 in the $Rb_7Mn_{12}Sb_{12}$-type structure, with the central atom

dx.doi.org/10.1021/ic401887b | *Inorg. Chem.* 2013, 52, 12682−12690

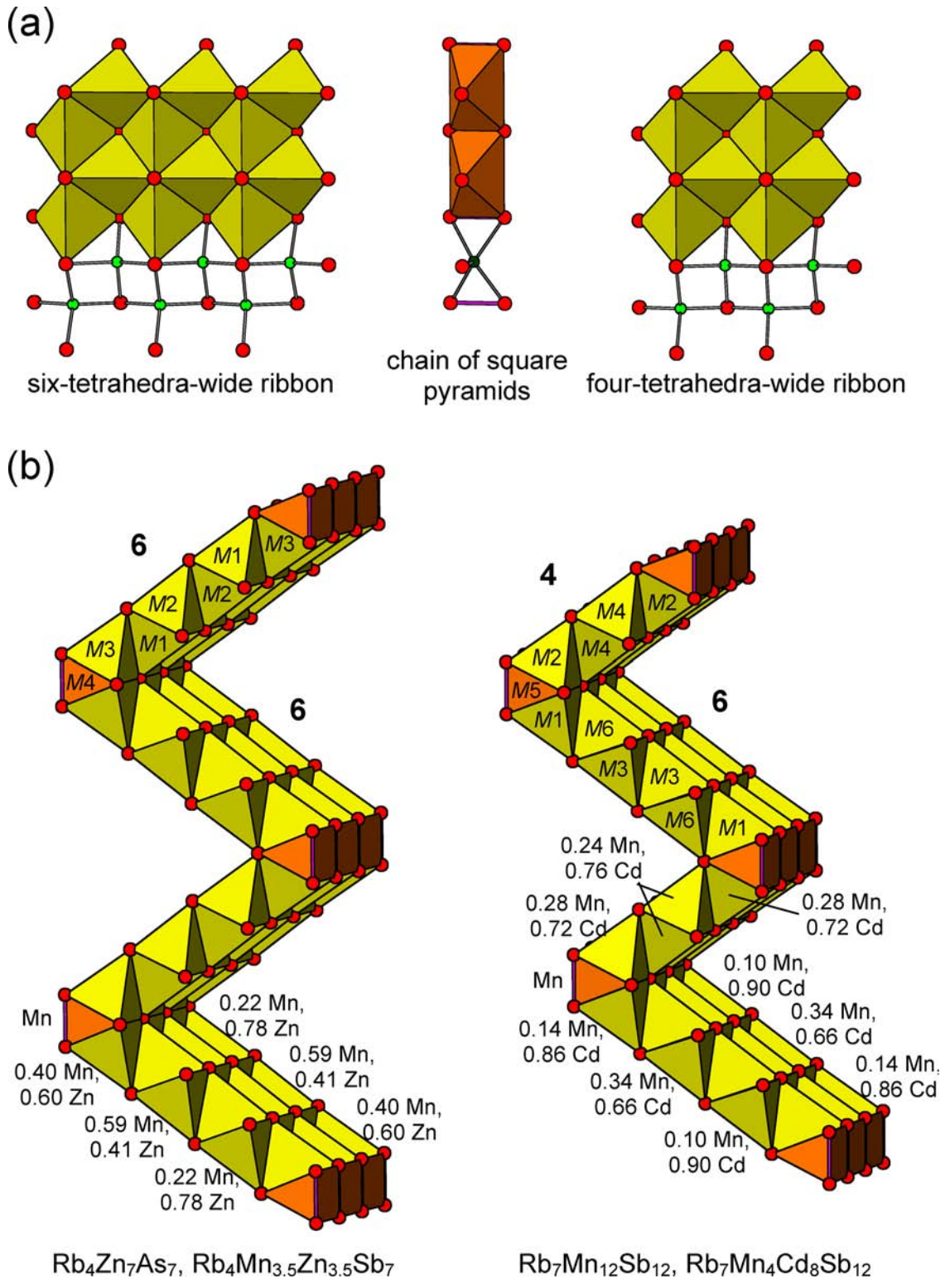

Figure 2. (a) Building units composed of edge-sharing M-centered tetrahedra or square pyramids. (b) Connectivity of building units to form the corrugated anionic layers found in the $Rb_4Zn_7As_7$-type (in 6−6−... sequence) and $Rb_7Mn_{12}Sb_{12}$-type structures (in 4−6−... sequence). Site occupancies for the M sites are shown for the quaternary derivatives $Rb_4Mn_{3.5}Zn_{3.5}Sb_7$ (left) and $Rb_7Mn_4Cd_8Sb_{12}$ (right).

displaced nearly on a quadrilateral face. Remarkably, there are no close contacts to any surrounding atoms above this face until another Rb atom about 5 Å away. The coordination geometry around Rb3 in the $Rb_4Zn_7As_7$-type structure and around Rb4 in the $Rb_7Mn_{12}Sb_{12}$-type structure appears at first glance to be approximately cubic (CN8). However, the distances to four of the eight surrounding As or Sb atoms are very long (more than 4 Å in the antimonides), so the coordination may be more properly described as [4 + 4]. In the course of the structure determination, it was noted that the displacement parameters for the As2 site in $Rb_4Zn_7As_7$ were elevated. This As2 site is common to the asymmetric

dx.doi.org/10.1021/ic401887b | Inorg. Chem. 2013, 52, 12682−12690

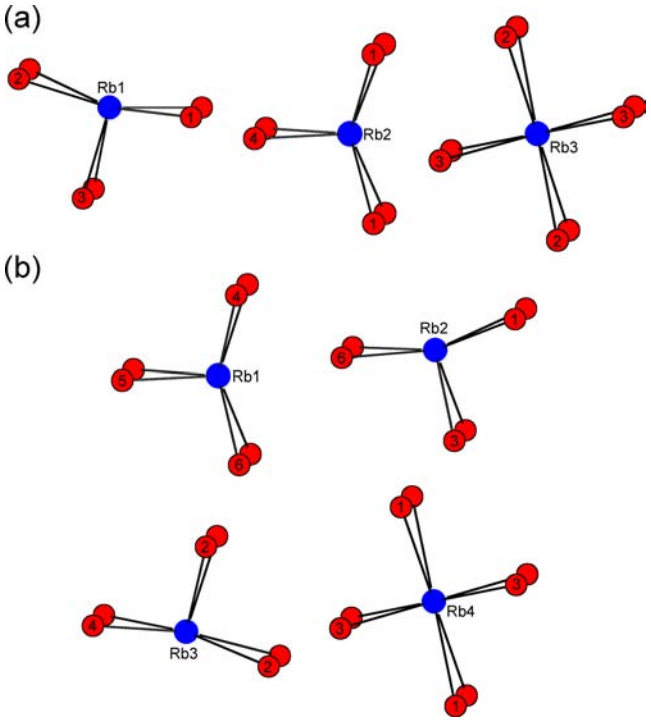

Figure 3. Coordination environments around Rb atoms in (a) $Rb_4Zn_7As_7$- and (b) $Rb_7Mn_{12}Sb_{12}$-type structures. Rb1 is coordinated to one of the atoms in the As_2 pair in the $Rb_4Zn_7As_7$-type structure; Rb2 and Rb3 are each coordinated to one of the atoms in the Sb_2 pair in the $Rb_7Mn_{12}Sb_{12}$-type structure.

coordination around Rb1 and the long distances to Rb3. Strong As−As homoatomic bonding develops to form an As_2 pair (2.36 Å), which is responsible for the distortion of the Mn-centered pyramids so that the base becomes compressed into a rectangle (Figure 2a). Close inspection of the displacement ellipsoids around the As2 site suggests a tendency to shift toward the open quadrilateral face of Rb1-centered trigonal prism, reducing the asymmetry, and to expand the As_2 pair. The As−As distance in this pair is close to some of the shortest values observed in other polyarsenides (e.g., 2.32−2.43 Å in Rb_3As_7, 2.38−2.48 Å in Rb_3As_{11}).[29,30] Vibrational spectroscopy to probe for the presence of this As−As pair would be interesting to perform, but is unfortunately precluded here because of the high air-sensitivity of the compounds. Similarly, Sb_2 pairs are present in the title antimonides, but the Sb−Sb distances (2.86−2.88 Å) are more typical of the median values found in many polyantimonides.[31] The Sb2 site in $Rb_4Mn_{3.5}Zn_{3.5}Sb_7$ also exhibits slightly more elevated displacement parameters, but the effect is less pronounced compared to the As2 site in $Rb_4Zn_7As_7$.

The structures resemble those of many other Zintl phases whose frameworks are built up by condensing tetrahedral units.[32] Normally, Zintl phases are electronically charge-balanced with closed-shell configurations for all atoms. Relatively rarely, however, electron-deficient (e.g., $Ba_5In_4Bi_5$)[33] or electron-excessive phases (e.g., $Ba_7Ga_4Sb_9$)[34,35] have been identified; they are interesting because they provide test cases for probing the limits of the Zintl concept. In the title compounds presented here, any reasonable assignment of charges leads to the conclusion of an electron deficiency. The transition-metal atoms (Mn, Zn, Cd) are assumed to be divalent. The Pn−Pn contacts within the Pn_2 pairs appear to correspond to normal single-bond distances, so these Pn atoms are assumed to be not fully reduced, each with a formal charge of 2−. The formulations $(Rb^+)_4(M^{2+})_7(h^+)(Pn^{2-})_2(Pn^{3-})_5$ and $(Rb^+)_7(M^{2+})_{12}(h^+)(Sb^{2-})_4(Sb^{3-})_8$, where h^+ represents a hole, suggests that these compounds are one electron short of complete charge balance. However, it is important to consider arguments that can be made against the presence of an electron deficiency. First, the electron deficiency could be eliminated if vacancies are introduced into some of the atom sites. In the only all-Zn compound prepared here, $Rb_4Zn_7As_7$, refinement of site occupancies suggests a substoichiometric model in which the Zn4 and As2 sites may be partially occupied. Nevertheless, the resulting formula, "$Rb_4Zn_{6.90(1)}As_{6.70(2)}$", still leads to an electron deficiency, albeit diminished, of 0.6 e^-. Second, the square pyramidal sites (M4 in the $Rb_4Zn_7As_7$-type and M5 in the $Rb_7Mn_{12}Sb_{12}$-type structures) are always the ones that are exlusively occupied by Mn-atoms in the quaternary derivatives ($Rb_4Mn_{3.5}Zn_{3.5}Sb_7$ and $Rb_7Mn_4Cd_8Sb_{12}$). It is tempting to assign Mn atoms that occupy these square pyramidal sites to be trivalent Mn^{3+} species, which would recover charge balance in the formulas. An appropriate basis for comparison is to ternary Mn-containing Zintl phases A−Mn−Sb (A = electropositive metal), for which AMnSb (A = Li−Cs),[6−8] $AMnSb_2$ (A = Ca, Sr, Ba),[36,37] AMn_2Sb_2 (A = Ca, Sr, Ba, Yb),[38−42] $A_{14}MnSb_{11}$ (A = Ca, Sr, Ba, Yb),[2−4,43] $A_{21}Mn_4Sb_{18}$ (A = Ca, Sr),[44−46] and $Yb_9Mn_{4+x}Sb_9$[47] are known. Except for $A_{14}MnSb_{11}$, all these compounds contain formally divalent Mn^{2+} species, in tetrahedral and sometimes square pyramidal coordination (in AMnSb). The case of $A_{14}MnSb_{11}$ is interesting: the initial assignment of trivalent Mn^{3+} species was subsequently overturned in favor of divalent Mn^{2+} species, as supported by X-ray magnetic circular dichroism measurements on $Yb_{14}MnSb_{11}$.[48] Comparison of Mn−Sb bond lengths does not provide much guidance because they fall in the same range (2.7−2.9 Å) among these compounds. Experimental measurements (such as magnetic susceptibility or X-ray spectroscopy) to probe the oxidation state of Mn in the title compounds would be helpful, but are hampered by their high air-sensitivity. There is growing consensus in the literature that high oxidation states for Mn are simply unlikely in antimonides.[41]

To investigate the electronic structure in more detail, band structure calculations were performed on the parent ternary compounds $Rb_4Zn_7As_7$ and $Rb_7Mn_{12}Sb_{12}$, for which the problem of metal site disorder can be avoided (Figure 4). Inspection of the density of states (DOS) curves shows that the Rb-based states are mostly empty and found well above the Fermi level; below the Fermi level, the Rb projection is not zero but is very small. As gauged by the integrated crystal orbital Hamilton population values (−ICOHP), the covalent portion of Rb−Pn bonding interactions is nearly negligible in both compounds (−ICOHP of 0.07 eV/bond for Rb−As contacts in $Rb_4Zn_7As_7$ and 0.05 eV/bond for Rb−Sb contacts in $Rb_7Mn_{12}Sb_{12}$). Thus, the usual notion is confirmed that the highly electropositive alkali-metal atoms tend to transfer their valence electrons to the rest of the anionic framework. The bonding around the [4 + 4]-coordinated Rb3 atoms in $Rb_4Zn_7As_7$ or the Rb4 atoms in $Rb_7Mn_{12}Sb_{12}$ can also be evaluated. In both compounds, the four longer Rb−Pn distances are confirmed to be essentially nonbonding (−ICOHP of <0.02 eV/bond) compared to the four shorter ones (−ICOHP of 0.07−0.08 eV/bond), suggesting that the coordination geometry should really be described as square planar.

dx.doi.org/10.1021/ic401887b | *Inorg. Chem.* 2013, 52, 12682−12690

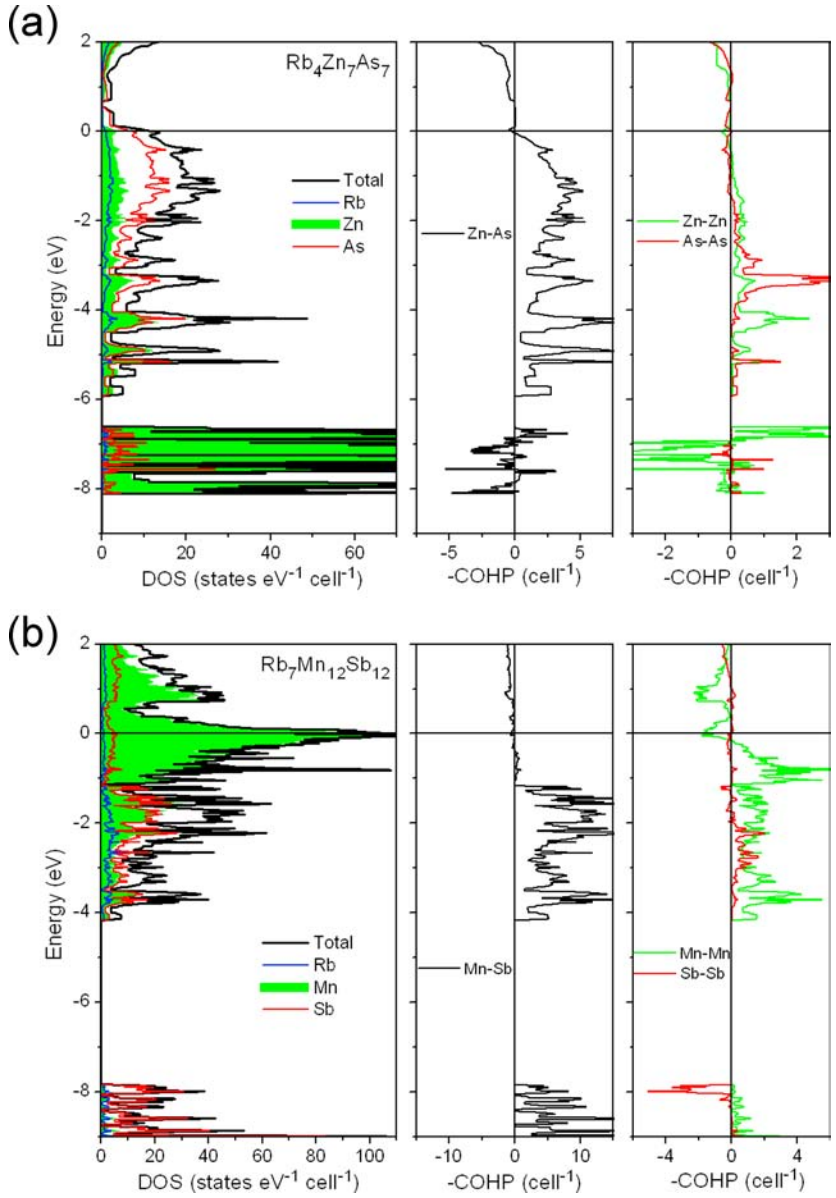

Figure 4. Density of states with atomic projections (left) and crystal orbital Hamilton population (COHP) curves (center and right) for (a) $Rb_4Zn_7As_7$ and (b) $Rb_7Mn_{12}Sb_{12}$. The horizontal line at 0 eV marks the Fermi level.

In $Rb_4Zn_7As_7$ (Figure 4a), the filled Zn 3d states are clustered mostly in a narrow band found well below the Fermi level, from −8 to −7 eV. The valence band appears as a wide manifold extending from −6 to +0.5 eV and results largely from mixing of Zn hybridized 4s/4p states with As 4p states; it is separated from the conduction band at higher energies by a small gap of 0.1 eV. The Zn−As bonding interactions are perfectly optimized up to the Fermi level, and they constitute the dominant contributions (>78% of the bonding energy in the entire structure), with an −ICOHP value of 1.11 eV/bond. The lowering of the Fermi level from the band gap at +0.5 eV to just below the top of the valence band at 0 eV corresponds precisely to the one-electron deficiency identified earlier. Interestingly, the origin of this electron deficiency is derived from As-based states, which constitute most of the DOS near the Fermi level. The occurrence of an As_2 pair in the structure results in bands that mimic the usual pattern of molecular orbitals for diatomic molecules. The σ_s and σ_s* levels are found very deep in energy at −13 and −10 eV (not shown). The bonding σ_p and π_p levels are separated from the antibonding π_p* and σ_p* levels at around −1.5 eV. The As−As COHP curve reveals the large bonding spike at −3.5 eV; the corresponding antibonding spike starts near +2 eV and maximizes at +3 eV above the scale shown. A singly bonded $(As_2)^{4-}$ pair is isoelectronic to a neutral diatomic halogen molecule in which only the σ_p* levels are unoccupied. The implication of the electron deficiency in $Rb_4Zn_7As_7$ is that the antibonding π_p* levels are slightly depopulated, which strengthens the As−As bond within this pair and accounts for the short 2.36 Å distance observed experimentally. The large −ICOHP value of 2.58 eV/bond for this As−As contact is also consistent with strong bonding. The other type of homoatomic bonding that could potentially occur in this structure comes from Zn−Zn contacts in the range 2.9−3.0 Å, presumably through so-called d^{10}−d^{10} interactions in which hybridization with s orbitals must be invoked.[49] Inspection of the Zn−Zn COHP curve confirms that some bonding is indeed present, but it is rather weak, with an −ICOHP value of 0.15 eV/bond.

dx.doi.org/10.1021/ic401887b | *Inorg. Chem.* 2013, 52, 12682−12690

In $Rb_7Mn_{12}Sb_{12}$, the electronic situation is quite different because the Mn component introduces a partially filled 3d-subshell, which the Fermi level cuts in the DOS (Figure 4b). Moreover, the gap between the valence and conduction bands has closed to become a pseudogap near +0.5 eV. The crystal field splitting experienced by Mn atoms, which are mostly in tetrahedral coordination geometries, is clearly manifested in the segregation of e and t_2 levels, the former mostly participating in Mn−Sb (−4 to −1 eV) and the latter in Mn−Mn bonding interactions (−1 eV upward), as seen in the COHP curves. As expected, the Mn−Sb interactions are strong (−ICOHP of 1.46 eV/bond), but now the Mn−Mn interactions also become significant (−ICOHP of 0.43 eV/bond). Sb−Sb interactions are present, with a similar pattern in the COHP curve as before (the σ_s* levels are now visible at −8 eV) and a resulting −ICOHP value of 1.37 eV/bond. It appears that the driving force for the electron deficiency is no longer the depletion of antibonding Sb−Sb levels, but rather Mn−Mn ones, which dominate near the Fermi level. Spin-polarized calculations will be important to perform to ascertain if the Mn-based states shift away from the Fermi level, depending on the magnetic properties yet to be determined for this compound.

The site preference (or "coloring problem") within the mixed-metal compounds $Rb_4Mn_{3.5}Zn_{3.5}Sb_7$ and $Rb_7Mn_4Cd_8Sb_{12}$ is not easy to rationalize. Apart from the existent compound $Rb_7Mn_{12}Sb_{12}$ which was already treated above, additional band structure calculations were performed on model compounds that would correspond to the ternary end-members of these quaternary systems but without changing the structural parameters, i.e., "$Rb_4Mn_7Sb_7$", "$Rb_4Zn_7Sb_7$", and "$Rb_7Cd_{12}Sb_{12}$" (Figure S3 in Supporting Information). The most straightforward way to assess site preferences is to compare the integrated electron densities within the Wigner−Seitz spheres surrounding specified atoms, called QVAL in the LMTO calculations performed here.[50] For the metal sites in $Rb_4Mn_7Sb_7$ and $Rb_4Zn_7Sb_7$, these values in decreasing order are (respectively for the two models): 6.78/11.76 for M4, 6.75/11.69 for M2, 6.72/11.54 for M1, and 6.56/11.47 for M3. Sites with higher QVAL are preferred by more electronegative atoms (or alternatively, by less easily ionized atoms), namely Zn in this case. However, the trend in QVAL is almost the reverse to the observed occupancy of Zn atoms in $Rb_4Mn_{3.5}Zn_{3.5}Sb_7$: 0.00 in M4, 0.41 in M2, 0.60 in M3, and 0.78 in M1. A similar assessment of QVAL for the metal sites in $Rb_7Mn_{12}Sb_{12}$ and $Rb_7Cd_{12}Sb_{12}$ also leads to inconsistency with the observed occupancies in $Rb_7Mn_4Cd_8Sb_{12}$. It would be helpful to perform higher-level calculations in which the total energies of alternative ordered model structures are compared. One crystal chemical principle which does seem to be respected is that more electronegative atoms prefer sites with lower CNs, accounting for the observation that the tetrahedral sites suffer from Mn/Zn or Mn/Cd disorder while the square pyramidal sites are restricted to Mn atoms only. Investigations of other members with different Mn:Zn or Mn:Cd ratios will also be important to understand trends in the site preferences and to establish limits of solid solubility.

CONCLUSIONS

Orthorhombic $Rb_4Zn_7As_7$ and monoclinic $Rb_7Mn_{12}Sb_{12}$ represent new structure types built up by connecting ribbons of edge-sharing metal-centered tetrahedra in different ways to generate corrugated anionic layers. This *aufbau* suggests possibilities for envisioning compounds belonging to homologous series in which the anionic layers contain analogous ribbons but of different widths. Given the preparation of quaternary mixed-metal derivatives $Rb_4Mn_{3.5}Zn_{3.5}Sb_7$ and $Rb_7Mn_4Cd_8Sb_{12}$, it will be necessary to evaluate the extent of the phase width and to target missing ternary end-members; these investigations may also shed light on the site preferences of transition-metal atoms. These syntheses may be challenging because there exist several compounds close in composition to the targeted compounds that may be more thermodynamically stable under the conditions used. The origin of the one-electron deficiency can be traced to the depopulation of antibonding Pn−Pn states in the $Rb_4Zn_7As_7$ or of antibonding M−M states in $Rb_7Mn_{12}Sb_{12}$; in effect, an internal oxidation of the Pn or M atoms takes place. Metallic behavior is predicted for these compounds. The Mn-containing compounds will be especially interesting to examine for their magnetic properties.

ASSOCIATED CONTENT

Supporting Information

X-ray crystallographic files in CIF format, additional crystallographic data, SEM images, EDX analyses, and additional DOS curves. This material is available free of charge via the Internet at http://pubs.acs.org.

AUTHOR INFORMATION

Corresponding Author

*E-mail: arthur.mar@ualberta.ca.

Notes

The authors declare no competing financial interest.

ACKNOWLEDGMENTS

This work was supported by the Natural Sciences and Engineering Research Council of Canada.

REFERENCES

(1) Kauzlarich, S. M. In *Chemistry, Structure, and Bonding of Zintl Phases and Ions*; Kauzlarich, S. M., Ed.; VCH: New York, 1996; pp 245−274.
(2) Fisher, I. R.; Wiener, T. A.; Bud'ko, S. L.; Canfield, P. C.; Chan, J. Y.; Kauzlarich, S. M. *Phys. Rev. B* **1999**, *59*, 13829−13834.
(3) Brown, S. R.; Kauzlarich, S. M.; Gascoin, F.; Snyder, G. J. *Chem. Mater.* **2006**, *18*, 1873−1877.
(4) Kauzlarich, S. M.; Brown, S. R.; Snyder, G. J. *Dalton Trans.* **2007**, 2009−2107.
(5) Juza, R.; Bohmann, T. *Z. Anorg. Allg. Chem.* **1961**, *308*, 159−178.
(6) Achenbach, G.; Schuster, H.-U. *Z. Anorg. Allg. Chem.* **1981**, *475*, 9−17.
(7) Bronger, W.; Müller, P.; Höppner, R.; Schuster, H.-U. *Z. Anorg. Allg. Chem.* **1986**, *539*, 175−182.
(8) Schucht, F.; Dascoulidou, A.; Müller, R.; Jung, W.; Schuster, H.-U.; Bronger, W.; Müller, P. *Z. Anorg. Allg. Chem.* **1999**, *625*, 31−36.
(9) Liu, Y.; Wu, L.-M.; Li, L.-H.; Du, S.-W.; Corbett, J. D.; Chen, L. *Angew. Chem., Int. Ed.* **2009**, *48*, 5305−5308.
(10) He, H.; Zevalkink, A.; Gibbs, Z. M.; Snyder, G. J.; Bobev, S. *Chem. Mater.* **2012**, *24*, 3596−3603.
(11) Madsen, G. K. H. *J. Am. Chem. Soc.* **2006**, *128*, 12148−12146.
(12) Toberer, E. S.; May, A. F.; Scanlon, C. J.; Snyder, G. J. *J. Appl. Phys.* **2009**, *105*, 063701-1−063701-5.
(13) Li, L.-H.; Chen, L.; Li, J.-Q.; Wu, L.-M. *Chem. Mater.* **2010**, *22*, 4007−4018.
(14) Yan, B.; Müchler, L.; Felser, C. *Phys. Rev. Lett.* **2012**, *109*, 116406-1−116406-5.
(15) Deng, Z.; Jin, C. Q.; Liu, Q. Q.; Wang, X. C.; Zhu, J. L.; Feng, S. M.; Chen, L. C.; Yu, R. C.; Arguello, C.; Goko, T.; Ning, F.; Zhang, J.; Wang, Y.; Aczel, A. A.; Munsie, T.; Williams, T. J.; Luke, G. M.;

Kakeshita, T.; Uchida, S.; Higemoto, W.; Ito, T. U.; Gu, B.; Maekawa, S.; Morris, G. D.; Uemura, Y. J. *Nat. Commun.* **2011**, *2*, 1425−1−1425−5.
(16) Zheng, W.-Z.; Wang, P.; Wu, L.-M.; Liu, Y.; Chen, L. *Inorg. Chem.* **2010**, *49*, 5890−5896.
(17) He, H.; Tyson, C.; Bobev, S. *Inorg. Chem.* **2011**, *50*, 8375−8383.
(18) Stoyko, S. S.; Khatun, M.; Mar, A. *Inorg. Chem.* **2012**, *51*, 9517−9521.
(19) He, H.; Stoyko, S. S.; Mar, A.; Bobev, S. *Acta Crystallogr., Sect. C* **2013**, *69*, 455−459.
(20) He, H.; Tyson, C.; Bobev, S. *Crystals* **2011**, *1*, 87−98.
(21) Khatun, M.; Stoyko, S. S.; Mar, A. *Inorg. Chem.* **2013**, *52*, 3148−3158.
(22) Saparov, B.; Saito, M.; Bobev, S. *J. Solid State Chem.* **2011**, *184*, 432−440.
(23) Saparov, B.; Broda, M.; Ramanujachary, K. V.; Bobev, S. *Polyhedron* **2010**, *29*, 456−462.
(24) Sheldrick, G. M. *SHELXTL, version 6.12*; Bruker AXS Inc.: Madison, WI, 2001.
(25) Gelato, L. M.; Parthé, E. *J. Appl. Crystallogr.* **1987**, *20*, 139−143.
(26) Tank, R.; Jepsen, O.; Burkhardt, A.; Andersen, O. K. *TB-LMTO-ASA Program, version 4.7*; Max Planck Institut für Festkörperforschung: Stuttgart, Germany, 1998.
(27) Lin, X.; Stoyko, S. S.; Mar, A. *J. Solid State Chem.* **2013**, *199*, 189−195.
(28) Pauling, L. *The Nature of the Chemical Bond*, 3rd ed.; Cornell University Press: Ithaca, NY, 1960.
(29) Emmerling, F.; Röhr, C. *Z. Naturforsch., B: J. Chem. Sci.* **2002**, *57*, 963−975.
(30) Emmerling, F.; Röhr, C. *Z. Anorg. Allg. Chem.* **2003**, *629*, 467−472.
(31) Papoian, G. A.; Hoffmann, R. *Angew. Chem., Int. Ed.* **2000**, *39*, 2408−2448.
(32) Eisenmann, B.; Cordier, G. In *Chemistry, Structure, and Bonding of Zintl Phases and Ions*; Kauzlarich, S. M., Ed.; VCH: New York, 1996; pp 61−137.
(33) Ponou, S.; Fässler, T. F.; Tobías, G.; Canadell, E.; Cho, A.; Sevov, S. C. *Chem.—Eur. J.* **2004**, *10*, 3615−3621.
(34) Alemany, P.; Alvarez, S.; Hoffmann, R. *Inorg. Chem.* **1990**, *29*, 3070−3073.
(35) Alemany, P.; Llunell, M.; Canadell, E. *Inorg. Chem.* **2006**, *45*, 7235−7241.
(36) Cordier, G.; Schäfer, H. *Z. Naturforsch., B: Anorg. Chem., Org. Chem.* **1977**, *32*, 383−386.
(37) Brechtel, E.; Cordier, G.; Schäfer, H. *J. Less-Common Met.* **1981**, *79*, 131−138.
(38) Brechtel, E.; Cordier, G.; Schäfer, H. *Z. Naturforsch., B: Anorg. Chem., Org. Chem.* **1979**, *34*, 921−925.
(39) Morozkin, A. V.; Isnard, O.; Henry, P.; Granovsky, S.; Nirmala, R.; Manfrinetti, P. *J. Alloys Compd.* **2006**, *420*, 34−36.
(40) Bobev, S.; Merz, J.; Lima, A.; Fritsch, V.; Thompson, J. D.; Sarrao, J. L.; Gillessen, M.; Dronskowski, R. *Inorg. Chem.* **2006**, *45*, 4047−4054.
(41) Xia, S.-Q.; Myers, C.; Bobev, S. *Eur. J. Inorg. Chem.* **2008**, 4262−4269.
(42) An, J.; Sefat, A. S.; Singh, D. J.; Du, M.-H. *Phys. Rev. B* **2009**, *79*, 075120-1−075120-6.
(43) Rehr, A.; Kuromoto, T. Y.; Kauzlarich, S. M.; Del Castillo, J.; Webb, D. J. *Chem. Mater.* **1994**, *6*, 93−99.
(44) Kim, H.; Condron, C. L.; Holm, A. P.; Kauzlarich, S. M. *J. Am. Chem. Soc.* **2000**, *122*, 10720−10721.
(45) Holm, A. P.; Olmstead, M. M.; Kauzlarich, S. M. *Inorg. Chem.* **2003**, *42*, 1973−1981.
(46) Xia, S.-Q.; Bobev, S. *Inorg. Chem.* **2007**, *46*, 874−883.
(47) Xia, S.-Q.; Bobev, S. *Chem. Mater.* **2010**, *22*, 840−850.
(48) Holm, A. P.; Kauzlarich, S. M.; Morton, S. A.; Waddill, G. D.; Pickett, W. E.; Tobin, J. G. *J. Am. Chem. Soc.* **2002**, *124*, 9894−9898.
(49) Jansen, M. *Angew. Chem., Int. Ed. Engl.* **1987**, *26*, 1098−1110.
(50) Misra, S.; Miller, G. J. *J. Am. Chem. Soc.* **2008**, *130*, 13900−13911.